

ApJ Supplement, in press

A Survey of Near Infrared Emission in Visual Reflection Nebulae

K. Sellgren^{1,2}

Department of Astronomy, Ohio State University, 174 West 18th Av., Columbus, OH
43210 USA

e-mail: sellgren@payne.mps.ohio-state.edu

M. W. Werner¹

M/S 169-327, Jet Propulsion Laboratory, California Institute of Technology, Pasadena, CA
91109

e-mail: mww@ipac.caltech.edu

L. J. Allamandola¹

M/S 245-6, NASA Ames Research Center, Moffett Field, CA 94035

¹Visiting astronomer at the Infrared Telescope Facility, operated by the University of Hawaii under contract with the National Aeronautics and Space Administration.

²Alfred P. Sloan Foundation Research Fellow

Abstract

We present a survey for extended $2.2\ \mu\text{m}$ emission in 20 new visual reflection nebulae, illuminated by stars with temperatures of 3,600 — 33,000 K. We detect extended $2.2\ \mu\text{m}$ emission in 13 new nebulae, illuminated by stars with temperatures of 6,800 – 33,000 K. For most of these 13 nebulae we have measured $J - K$, $H - K$, and $K - L'$, as well as obtaining surface brightness measurements at the wavelength of the $3.3\ \mu\text{m}$ emission feature. All of the reflection nebulae with extended near infrared emission in excess over scattered starlight have very similar near infrared colors and show the $3.3\ \mu\text{m}$ feature in emission with similar feature-to-continuum ratios. The $3.3\ \mu\text{m}$ feature-to-continuum ratio ranges from ~ 3 to ~ 9 , both within individual nebulae and from nebula to nebula, which suggests that the $3.3\ \mu\text{m}$ feature and its underlying continuum arise from different materials, or from different ranges of sizes within a size distribution of particles. No dependence on the temperature of the illuminating star is seen in the near infrared colors or $3.3\ \mu\text{m}$ feature-to-continuum ratio, over a factor of two in stellar temperature. This is similar to our previous IRAS results, in which we found no dependence of the ratio of $12\ \mu\text{m}$ to $100\ \mu\text{m}$ surface brightnesses in reflection nebulae illuminated by stars with temperatures of 5,000–33,000 K.

Subject headings: ISM: dust, extinction – ISM: molecules – ISM: reflection nebulae – infrared: general – infrared: interstellar: continuum – infrared: interstellar: lines

1. Introduction

Extended near infrared continuum emission in visual reflection nebulae was discovered by Sellgren, Werner, & Dinerstein (1983; hereafter Paper I) and Sellgren (1984; hereafter Paper II) in NGC 2023, NGC 2068, and NGC 7023. They showed that this near infrared continuum emission, unlike the visual reflection nebulosity, was not primarily due to scattered starlight. Sellgren, Werner, & Dinerstein (1992; hereafter Paper IV) quantified the amount of near infrared scattered starlight in NGC 2023 and NGC 7023 by polarization observations, and showed that it contributes $<20\%$ of the observed $2.2 \mu\text{m}$ surface brightness of NGC 7023. It was also shown in Papers I and II that thermal emission from dust grains in equilibrium with the stellar radiation field is unable to account for the near infrared continuum emission. Observations of visual reflection nebulae by Sellgren et al. (1985), Castelaz, Sellgren, & Werner (1987), Sellgren, Luan, & Werner (1990; hereafter Paper III), and Roche, Aitken, & Smith (1994) show that this infrared continuum emission extends at least from 1 to $25 \mu\text{m}$.

A variety of proposals have been made to explain this near infrared continuum emission. One idea is thermal emission from transiently heated tiny grains, with a radius of $\sim 10 \text{ \AA}$, which are briefly heated to temperatures near $\sim 1000 \text{ K}$ by the absorption of single ultraviolet (UV) photons (Papers I and II). Another suggestion is a quasi-continuum of overlapping overtone and combination bands arising from vibrational fluorescence in polycyclic aromatic hydrocarbon (PAH) molecules (Léger & Puget 1984; Allamandola, Tielens, & Barker 1985). A third explanation is an electronic fluorescence in PAH molecules (Allamandola, Tielens, & Barker 1989).

The near infrared continuum emission in the visual reflection nebulae NGC 2023, NGC 2068, and NGC 7023 is strongly associated with an emission feature at $3.3 \mu\text{m}$ (Paper I). This emission feature has also been detected in the visual reflection nebulae NGC 1333 (Whittet et al. 1983) and Parsamyan 18 (Jourdain de Muizon, d’Hendecourt, & Geballe 1990). The $3.3 \mu\text{m}$ feature is one of a group of emission features at 3.3, 6.2, 7.7, 8.6, and $11.3 \mu\text{m}$, observed together in proto-planetary nebulae, planetary nebulae, reflection nebulae, H II regions, young stellar objects, and galaxies dominated by star formation (see Aitken 1981, Willner 1984, Bregman 1989, Puget & Léger 1989, and Allamandola, Tielens, & Barker 1989 for reviews). The 6.2, 7.7, 8.6, and $11.3 \mu\text{m}$ features have also been detected in the visual reflection nebulae NGC 7023 (Sellgren et al. 1985), NGC 2023 (Sellgren et al. 1985; Roche, Aitken, & Smith 1994), Parsamyan 18 (Cohen, Tielens, & Allamandola 1985; Cohen et al. 1986), NGC 2071 (Cohen et al. 1986), and NGC 1333 (Roche, Aitken, & Smith 1994).

The emission features seen at 3.3, 6.2, 7.7, 8.6, and 11.3 μm are generally believed to be due to some sort of aromatic hydrocarbon. Proposed laboratory analogs for the material which emits these features include amorphous carbon (Duley & Williams 1981; Borghesi, Bussoletti, & Colangeli 1987), $\text{C}_{60}\text{H}_{60}$ (Webster 1991), coal (Papoular et al. 1989), hydrogenated amorphous carbon (Blanco, Bussoletti, & Colangeli 1988; Ogmen & Duley 1988), nitrogenated amorphous carbon (Saperstein, Metin, & Kaufman 1989), the carbonaceous residue from Orgueil meteorite (Wdowiak, Flickinger, & Cronin 1988), polycyclic aromatic hydrocarbons (Léger & Puget 1984; Allamandola, Tielens, & Barker 1985, 1989; Léger, d’Hendecourt, & Défourneau 1989), quenched carbonaceous composite (Sakata et al. 1987), and a spiral carbonaceous microparticle with an internal hydrogen (Balm & Kroto 1990). Most of these proposed laboratory analogs identify the 3.3 μm feature with a C–H stretch vibration in aromatic hydrocarbons. The emission mechanism for the aromatic hydrocarbon features has been proposed to be thermal emission from transiently heated tiny aromatic grains (Papers I and II), or a vibrational fluorescence in PAH molecules (Léger & Puget 1984; Allamandola, Tielens, & Barker 1985, 1989). Although similar materials and mechanisms have been proposed in each case, the emitting material and emission mechanism for the 3.3 μm feature and the adjacent continuum may, or may not, be the same.

We present here the results of a survey of 20 additional visual reflection nebulae for extended near infrared continuum emission. Our goal is to increase the sample of visual reflection nebulae for which near infrared surface brightnesses and colors are available, in order to see whether the three bright nebulae observed in Papers I and II are typical or extraordinary visual reflection nebulae. We also present the results of a search for accompanying 3.3 μm emission whenever extended near infrared continuum emission is detected. We compare our observations to observations at visual wavelengths, in order to quantify any possible contribution from scattered starlight to the near infrared continuum emission. We chose reflection nebulae with a range of values for T_{star} , the temperature of the central illuminating star, to determine if there was any dependence of the near infrared emission properties on T_{star} . Our sample was primarily chosen from the survey of visual reflection nebulae conducted by van den Bergh (1966). Table 1 gives a list of the nebulae we have observed, and summarizes the properties of the central illuminating star for each nebula.

2. Observations

The near infrared observations were primarily obtained at the NASA Infrared Telescope Facility at Mauna Kea Observatory, between 1984 and 1988. Observations were also obtained at the United Kingdom Infrared Telescope and at the University of Hawaii 2.2-m telescope at Mauna Kea Observatory in 1984, and at the 0.6-m telescope at Mount Wilson Observatory in 1981. The observational setup was the same as in Papers I and II. Single detector InSb photometer systems cooled to solid nitrogen temperatures were used in all cases. For two nebulae, NGC 2071 and Parsamyan 18, 3.2–3.6 μm spectra were obtained with a circular variable filter (CVF) having a spectral resolution $\lambda/\Delta\lambda = 67$, and a 10.5'' diameter beam. For the remaining sources studied at 3.3 μm , however, we do not have complete spectra near the feature, but only have photometry at the wavelength of the 3.3 μm feature, obtained with CVFs having spectral resolutions of $\lambda/\Delta\lambda = 50$ –100. In these cases we estimated the continuum near the 3.3 μm feature by interpolation between K (2.2 μm) and L' (3.8 μm) surface photometry.

Chopping secondary mirrors were used for sky subtraction, except for the 1981 observations where the focal plane chopper described by Becklin and Neugebauer (1968) was used. The values used for the chopper throw for each nebula are listed in Table 2.

The observational approach to this study of extended near infrared emission in reflection nebulae was to search first for emission at K at several nebular positions, typically 42'' from the star. Positions obviously contaminated by field stars in the signal or reference beam were eliminated, and if K emission was detected in the remaining positions, the brightest of these positions was selected for further study. Observations were obtained at this brightest position with a smaller aperture to test whether the emission was truly extended, then as much data as time permitted were obtained at the brightest position at J (1.25 μm), H (1.65 μm), L' , and, using the CVF, at the wavelength of the 3.3 μm emission feature. For a few nebulae, multiaperture photometry at K or single aperture photometry at other infrared wavelengths were obtained at more than one nebular position.

Because the observations entailed a search for faint extended emission near bright stars, careful measurements were made of the instrumental scattered light. Each offset position measured in a nebula was also measured near a bright standard star, and the scattered light correction determined for each night applied to the observations of the reflection nebulae. At the standard offset positions given in Table 3a, the difference, Δm , between the magnitude of a star and the magnitude of the instrumental scattered light correction measured in a 10.5'' diameter aperture ranged from $\Delta m = 8.7$ mag to $\Delta m = 12.6$ mag on different nights and at different positions, with a typical uncertainty in Δm at a given position and night of 0.3 mag. The resulting instrumental scattered light correction was negligible for the brightest nebulae, but was equal to or larger than the nebular emission at some positions

within vdB 10, vdB 16, 23 Tau, Elias 1, vdB 34, vdB 35, vdB 46, vdB 101, vdB 111, vdB 133, vdB 135, and IC 5076. The uncertainties given for the observations therefore include both the statistical and photometric uncertainties in the individual observations, and the uncertainties in the instrumental scattered light corrections. For many nebulae in which no emission was detected, particularly those with bright illuminating stars, our observed upper limits are dominated by the uncertainty in the instrumental scattered light correction rather than by the combination of statistical and photometric uncertainties.

Photometry was also obtained for the central stars of many of the nebulae in Table 1, at J , H , K , L' , N ($10\ \mu\text{m}$), Q ($20\ \mu\text{m}$), and, using the CVF, at the wavelength of the $3.3\ \mu\text{m}$ feature. The J , H , K , and L' stellar photometry was usually obtained at the same time as the surface photometry of the surrounding nebula, with the same observing setup, as part of determining the instrumental scattered light correction. The N and Q photometry was obtained at the IRTF in 1987, using a standard single-channel bolometer system cooled with liquid helium, and a $6''$ diameter aperture.

All observations were obtained on photometric nights. The photometry and spectrophotometry were calibrated by observations of stars from the IRTF standard star list (Tokunaga 1986), with stars from Elias et al. (1982) and the Caltech unpublished list preferred. We assumed fluxes for zero magnitude of 1630 Jy, 1050 Jy, 655 Jy, 313 Jy, and 248 Jy at J , H , K , $3.3\ \mu\text{m}$, and L' respectively, which were adopted from or interpolated between the values of Cohen et al. (1992). Scans of bright stars were used to correct the photometry of extended sources for the difference between a point source and uniform extended source. This correction was not included in Paper I, and so we have applied this correction to the results of Paper I when they are given for comparison with the new results of the present paper.

3. Results

3.1. K surface photometry

The results of the K surface brightness photometry are given in Table 3. Table 3*a* gives surface brightnesses measured at standard offsets from the central star, of $30''\text{E } 30''\text{N}$, $30''\text{E } 30''\text{S}$, $30''\text{W } 30''\text{N}$, and $30''\text{W } 30''\text{S}$. In Table 3*b* we present K surface brightnesses measured at other offsets, generally chosen to complement data available at other wavelengths. We include in Table 3 results from Paper I for NGC 2023, NGC 2068, and NGC 7023, corrected

for an improved calibration, plus some new observations of these sources. Observations for 20 additional visual reflection nebulae are presented here, which combined with the results of Paper I provides K surface brightnesses for 23 sources.

Of the 20 new nebulae observed, extended K emission was clearly detected in 13 of them. Emission at K at offsets away from the central star was seen in two other nebulae, vdB 135 and IC 5076, but observations with different beam sizes were either unavailable or were unable to clearly establish that the emission was extended. No correction was attempted for possible emission in the reference beam, which is a potential problem for the most extended sources, particularly 23 Tau. For each nebula we combined all observations at the same nebular offset, wavelength, and aperture size, without regard for differences in the chopper amplitude or direction.

3.2. Nebular Colors

In Table 4 we present the colors of the reflection nebulae, at J , H , K , and L' . We include for comparison the colors of the three nebulae presented in Paper I, NGC 7023, NGC 2023, and NGC 2068, again corrected for an improved calibration, plus some new observations of these sources. Some nebular colors were measured at multiple spatial positions, or at the same spatial position but with different aperture sizes. Measurements of, or lower limits to, $J - K$ and $H - K$ were obtained for all 15 nebulae in Table 4. Measurements of, or upper limits on, $K - L'$ were obtained for 14 of the 15 nebulae in Table 4.

3.3. The 3.3 μm feature

For two nebulae, NGC 2071 and Parsamyan 18, 3.2–3.6 μm spectra were obtained with a CVF. Our spectrum of NGC 2071 is presented in Figure 1. Our spectrum of Parsamyan 18, which is not shown, is similar to the spectrum of this source published by Jourdain de Muizon et al. (1990). We did not have time for complete 3.2–3.6 μm spectra of additional sources, so for the brightest reflection nebulae photometry was obtained at the wavelength of the 3.3 μm feature, using the CVF. These observations are included in Table 4, in the form of a difference between K and the observed 3.3 μm magnitude. Measurements of, or upper limits on, $K - [3.3 \mu\text{m}]$ were obtained for 14 of the 15 nebulae in Table 4.

3.4. Photometry of the Central Stars

In Table 5 we present the near-infrared magnitudes we have measured for the central stars of the reflection nebulae in this paper. Magnitudes are given at J , H , K , and L' , and at the wavelength of the $3.3 \mu\text{m}$ feature as measured through the CVF.

Some central stars have an intrinsic $3.3 \mu\text{m}$ emission feature. The spectrum of the pre-main sequence star Elias 1 shows emission features at 3.3 , 3.43 , and $3.53 \mu\text{m}$ (Allen et al. 1982; Whittet et al. 1983; Whittet, McFadzean, & Geballe 1984; Schutte et al. 1990; Tokunaga et al. 1991). The $3.3 \mu\text{m}$ feature is detected in $\sim 20\%$ of Herbig Ae/Be stars, and the $3.53 \mu\text{m}$ feature is detected in $\sim 5\%$ of Herbig Ae/Be stars (Brooke, Tokunaga, & Strom 1993). The $3.3 \mu\text{m}$ feature is not detected toward the central stars of NGC 7023 (Paper II) and NGC 1999 (Brooke et al. 1993), which are both Herbig Ae/Be stars.

Other central stars show a $3.3 \mu\text{m}$ emission feature due to nebular contamination, because the aperture photometry for these stars contains significant contributions from the surrounding nebula included in the measurement. This effect was seen in Paper II, where the CVF spectrum of the central star of NGC 2023 showed the $3.3 \mu\text{m}$ feature in emission. The central stars of NGC 1333 and Parsamyan 18, and probably the central stars of NGC 2023, vdB 74, and NGC 7129, have a measured magnitude at $3.3 \mu\text{m}$ which is brighter than either the K or L' magnitude, or which depends on aperture size. The central stars of Parsamyan 18 and NGC 7129 are Herbig Ae/Be stars without published $3 \mu\text{m}$ spectra, but a comparison of their infrared magnitudes and the surface brightness of the surrounding nebula indicates that any $3.3 \mu\text{m}$ emission toward these stars would be most likely due to nebular contamination rather than intrinsic emission from the star.

In Table 6 we present the mid-infrared magnitudes we have measured for the central stars of the reflection nebulae in this paper. Magnitudes at 10 and $20 \mu\text{m}$ (N and Q respectively) are given. We do not use these observations in our analysis but present them for completeness.

4. Discussion

4.1. Energy Distributions

In Paper II the observed broad-band energy distributions from 1 to $1000 \mu\text{m}$ were presented for three reflection nebulae, NGC 2023, NGC 2068, and NGC 7023. These energy

distributions show a strong near-infrared excess over the expected level of near-infrared scattered starlight, mid-infrared emission which is even stronger than the near-infrared emission, and a peak in the far infrared presumably due to thermal emission from grains in equilibrium with the radiation field. In Paper III the IRAS energy distributions from 12 to 100 μm were shown to be very similar for a sample of reflection nebulae illuminated by stars with widely varying T_{star} . In Figure 1 we plot the 0.44–3.8 μm broad-band energy distribution of one of our observed reflection nebulae, NGC 2071, along with its spectrum near the 3.3 μm feature. Its visual and near infrared energy distribution is very similar to that of previously observed reflection nebulae. Its 3.2–3.6 μm spectrum is also very similar to that of previously observed reflection nebulae (Paper I; Whittet et al. 1983; Jourdain de Muizon et al. 1990).

For comparison with the observed nebular emission of NGC 2071, we have estimated the scattered starlight for NGC 2071, to show that while the visual emission is primarily scattered starlight, the infrared emission is well in excess of the expected scattered starlight. We predicted the amount of surface brightness, S , of scattered starlight, relative to the stellar flux, F_{star} , using the model of Witt (1985a), and assumed that all of the observed nebular emission at V is due to scattered starlight. The prediction for the color of S/F_{star} between two wavelengths λ_1 and λ_2 in Equation 2 of Witt (1985a) is

$$\frac{(S/F_{\text{star}})_{\lambda_1}}{(S/F_{\text{star}})_{\lambda_2}} = \frac{\omega(\lambda_1) [1 - e^{-\tau_0(\lambda_1)}] \exp[\tau_2(\lambda_1) - \tau_1(\lambda_1)]}{\omega(\lambda_2) [1 - e^{-\tau_0(\lambda_2)}] \exp[\tau_2(\lambda_2) - \tau_1(\lambda_2)] p(\lambda_1, \lambda_2)}, \quad (1)$$

where $\tau_0(\lambda)$ is the optical depth along the observed line of sight through the nebula, $\tau_1(\lambda)$ is the optical depth from the star to the nebular position observed, $\tau_2(\lambda)$ is the nebular optical depth from the star to the observer, $\omega(\lambda)$ is the albedo, and p is a factor which depends on the nebular geometry and the wavelength dependence of the phase function asymmetry. We set $\tau_2 = 0.5\tau_0$, $\tau_1 = 0$, and $p = 1$ for simplicity. With these assumptions, the results are not sensitive to the adopted value of τ_0 as long as it is not much more than 1, the regime in which the approximations made by Witt (1985a) break down. We adopted the extinction law of Mathis (1990). Theoretical and observational estimates of $\omega(K)$ range from 0.21 to > 0.8 (Draine & Lee 1984; Kim, Martin, & Hendry 1994; Witt et al. 1994). We have adopted two values for $\omega(\lambda)$, a low albedo value (Draine & Lee 1984) and a high albedo value in which the albedo is independent of wavelength from 0.44 to 3.8 μm . We calculated the predicted scattered light with both high and low values of the albedo. Our results are shown in Figure 1, which demonstrates that at wavelengths longer than 1 μm scattered starlight is not a significant contribution to the observed emission of NGC 2071, for either assumption about the albedo.

4.2. Nebular Colors

The colors of the reflection nebulae are all very similar, in close agreement with the energy distribution of the nebulae whose observations are presented in Paper I. In Figure 2 we show a plot of $J - H$ vs. $H - K$ for the nebulae, to illustrate their similarity among nebulae. All nebular positions for which we have $J - H$ and $H - K$ colors are plotted. Nebulae in which the $3.3 \mu\text{m}$ feature was detected are shown as filled circles, while nebulae in which the $3.3 \mu\text{m}$ feature was not searched for, or searched for and not detected, are shown as open circles. We also show the colors of the central stars, with open stars for normal stars and filled stars for stars with emission lines and thus a probable infrared excess.

The reflection nebulae all have near infrared colors redder than their illuminating stars, with the exceptions of AE Aur, vdB 10, and NGC 1999. These nebulae are the bluest nebulae in Figure 2. The remaining nebulae in Figure 2 all have infrared colors which are typical of the three reflection nebulae studied in Papers I and II, and which characterize the energy distribution of tiny grain and/or PAH continuum emission. Thus the three reflection nebulae studied in Papers I and II, chosen for their high surface brightness, are very representative of the larger sample of reflection nebulae studied in the present paper.

A determination of the typical $V - K$ color of reflection nebulae dominated by tiny grain and/or PAH emission is useful for estimating the expected infrared surface brightness of reflection nebulae for which only optical observations exist, or the expected visual surface brightness of reflection nebulae for which only infrared observations exist. We have constructed $V - K$ colors for the nebulae for which visual surface brightnesses were available at positions near the positions observed in the near infrared (Racine 1971; Witt 1977; Witt & Cottrell 1980a; Cottrell 1981; Witt, Schild, & Kraiman 1984; Witt 1985b, 1986; Witt & Schild 1986; Witt et al. 1987). In Figure 3 we plot the $V - K$ color of the nebula, $(V - K)_{\text{neb}}$, vs. the observed $V - K$ color of the central star, $(V - K)_{\text{star}}$. As in Figure 2, all nebular positions with $V - K$ colors are plotted, with nebulae in which the $3.3 \mu\text{m}$ feature was detected shown as filled circles, and nebulae in which the $3.3 \mu\text{m}$ feature was not searched for, or searched for and not detected, shown as open circles. Note that the observed stellar $V - K$ color is sometimes considerably redder than expected for the observed $E(B - V)$ and spectral type, because several stars in our nebulae are Herbig Ae/Be stars with intrinsic infrared excesses (Elias 1, V380 Ori, star A in Parsamyan 18, HD 200775, and BD +65 1637). The nebulae with detected $3.3 \mu\text{m}$ emission features all have $(V - K)_{\text{neb}} > 1.7$, independent of $(V - K)_{\text{star}}$. NGC 1999 and 23 Tau have significantly bluer $(V - K)_{\text{neb}}$ colors compared to the nebulae with detected $3.3 \mu\text{m}$ feature emission.

4.3. Scattered Starlight

The fact that NGC 1999 has near infrared colors significantly bluer than its illuminating star, and that AE Aur and vdB 10 have near infrared colors similar to their illuminating stars, suggests the possibility that in these particular sources the near infrared emission could have a reflected starlight component. In Paper IV the near infrared colors of the reflected starlight component in NGC 7023 were observed to be extremely blue compared to the colors of the illuminating star, consistent with predictions for Rayleigh scattering in an optically thin nebula: $\Delta(J - H) = -1.21$ and $\Delta(H - K) = -1.25$, where the difference is in the sense of the color of the nebula minus the color of the star. If we adopt a Mathis (1990) extinction law, then Equation 1 predicts $\Delta(J - H) = -0.79$ and $\Delta(H - K) = -1.03$ for a low infrared albedo (from Draine & Lee 1984), and $\Delta(J - H) = -0.51$ and $\Delta(H - K) = -0.53$ for a high infrared albedo (albedo independent of wavelength). NGC 1999 is observed to have $\Delta(J - H) = -0.77$ and $\Delta(H - K) = -0.84$, colors which are within the range of predictions for purely scattered starlight in an optically thin nebula.

The relative amount of visual and near infrared nebular emission, as measured by a color such as $V - K$, is another measure of the relative importance of scattered starlight and emission from tiny grains and/or PAH molecules. The observed $V - K$ color of the central star, $(V - K)_{\text{star}}$, depends on the reddening of the star, which for many nebular geometries is similar to the reddening of the nebula, and on T_{star} . The observed nebular $V - K$ color, $(V - K)_{\text{neb}}$, depends on $(V - K)_{\text{star}}$, on any differential reddening between nebula and star which is usually much smaller than the total reddening, and on the relative contributions of scattered starlight and emission from tiny grains and/or PAH molecules to the infrared emission. Since the visual nebular emission is entirely due to scattered starlight, the $V - K$ color should be smaller for nebulae with infrared emission due only to scattered starlight, and larger for nebulae with both excess infrared emission and infrared scattered starlight.

We have drawn lines on Figure 3 for $(V - K)_{\text{neb}}$ as a function of $(V - K)_{\text{star}}$ for scattered starlight, as predicted by Equation 1, for four simple cases: (1) $\tau_0(K)/\tau_0(V) = 1$ and $\omega(K)/\omega(V) = 1$ (optically thick nebula, high albedo grains); (2) $\tau_0(K)/\tau_0(V) = 1$ and $\omega(K)/\omega(V) = 0.38$ (optically thick nebula, low albedo grains); (3) $\tau_0(K)/\tau_0(V) = 0.11$ and $\omega(K)/\omega(V) = 1$ (optically thin nebula, high albedo grains); and (4) $\tau_0(K)/\tau_0(V) = 0.11$ and $\omega(K)/\omega(V) = 0.38$ (optically thin nebula, low albedo grains). For optically thin nebulae the value of $\tau_0(K)/\tau_0(V)$ is from Mathis (1990). We predict $(V - K)_{\text{neb}} - (V - K)_{\text{star}} = 0.00, -1.06, -2.42, \text{ and } -3.49$, respectively for Cases (1), (2), (3), and (4). Nebulae with K emission in excess of scattered starlight fall above and to the left of these lines.

All of the nebulae with detected $3.3 \mu\text{m}$ emission in Figure 3 (shown as filled circles)

fall above and to the left of the lines for Cases (3) and (4), and most fall above and to the left of the line for Case (2). Note that the measurements of scattered starlight in NGC 7023 from the polarization results of Paper IV fall between the lines for Case (2) and Case (4). NGC 1999 also falls in this region, again suggesting its K emission is primarily scattered starlight from an optically thin nebula.

Surface brightness measurements at V are not available for many of our reflection nebulae, particularly those illuminated by cooler stars, and we did not obtain near infrared colors for nebulae which we did not detect at K . We therefore make an estimate of the surface brightness of scattered starlight at K , $S_{\text{ref}}(\text{est})$, in order to compare our measurements of and upper limits on the observed K surface brightness, S_{obs} , for our entire sample of reflection nebulae. The surface brightness of an optically thin reflection nebula (Paper IV) is

$$S_{\text{ref}} = \frac{\tau \omega F_{\text{star}} H(g, \theta) \sin^2 \theta}{4\pi \phi^2} . \quad (2)$$

In this equation, τ is the extinction optical depth, ω is the grain albedo, F_{star} is the observed flux of the star, and ϕ is the angular offset between star and nebula. The star and nebula are assumed to be reddened by the same amount in this equation. The angular dependence of scattering is characterized by the phase function $H(g, \theta)$, where $g = \langle \cos \theta \rangle$ is the phase asymmetry parameter and θ is the scattering angle; the functional form of $H(g, \theta)$ is given by Henyey & Greenstein (1941). This surface brightness, when maximized with respect to the scattering angle and phase function (Sellgren 1983), becomes

$$S_{\text{ref}}(\text{est}) = \frac{\tau \omega F_{\text{star}}}{4\pi \phi^2} . \quad (3)$$

Thus $S_{\text{obs}}/S_{\text{ref}}(\text{est}) > 1$ is a clear indication of nebular emission from something other than reflected light.

We use two techniques to estimate a value of $\tau(K)$ to use in Equation 3. First we use the value of $A_V(\text{neb})$ derived in Paper III, which is an estimate of $\tau(V)$ for each nebula calculated from the amount of starlight incident on the nebula which is reradiated in the far infrared. Second we use Equation 3 combined with visual observations of reflected light (Racine 1971; Witt 1977; Witt & Cottrell 1980a; Cottrell 1981; Witt, Schild, & Kraiman 1984; Witt 1985b, 1986; Witt & Schild 1986; Witt et al. 1987) to estimate $\tau(V)$ for each nebula. The value of $\tau(V)$ was calculated from visual observations at, or very near, each measured infrared position. For IC 5076, we extrapolated data at offsets of 50'' and 100'' to a radius of 42''. We then use a standard extinction curve (Mathis 1990) to estimate $\tau(K) = \tau(V) / 9.29$. We adopted a high infrared albedo, i.e. assumed the albedo was independent of wavelength. Our estimates of $\tau(K)$ are given in Table 7.

We plot our derived values of $S_{\text{obs}}/S_{\text{ref}}(\text{est})$ vs. T_{star} in Figure 4. All nebular positions with K data and an estimate of $\tau(V)$ are shown. If multiaperture data were not able to demonstrate the K emission is extended, that detection was treated as an upper limit. Nebulae in which the $3.3 \mu\text{m}$ feature was detected are shown in Figure 4 as filled circles, while nebulae in which the $3.3 \mu\text{m}$ feature was not searched for, or searched for and not detected, are shown as open circles. Open triangles mark the reflected light measurements in NGC 7023 (Paper IV). We plot two independent points for nebulae in which there were both IRAS estimates of $A_V(\text{neb})$ from Paper III and visual surface photometry of the nebula from which to estimate $\tau(V)$. These estimates agree to a factor of 3 on average, which provides an estimate of our uncertainty in $\tau(V)$.

Figure 4 shows that most nebulae have an observed K surface brightness which is above the expected amount of reflected starlight we have estimated. The only K surface brightnesses low enough to be consistent with purely scattered starlight are the measurements of NGC 1999 and the upper limits on vdB 35, vdB 101, and vdB 135. The observed surface brightness of reflected light in NGC 7023 (Paper IV) is also consistent with the expected surface brightness of reflected light, which is a check on our technique. IC 5076 and Ced 201, whose upper limits correspond to high K surface brightnesses, could have K surface brightnesses which are lower than our upper limits, and thus we cannot rule out these nebulae having K surface brightnesses which are also consistent with being due to scattered starlight.

We conclude that the K extended emission we detect is due to something other than reflected starlight in most of our nebulae. While the K surface brightness of NGC 1999 is consistent with predicted levels of scattered starlight, *all* of the remaining sources detected at K are strong candidates for tiny grain and/or PAH emission at K .

4.4. The $3.3 \mu\text{m}$ feature

All of the sources where the $3.3 \mu\text{m}$ feature was detected are characterized by K surface brightnesses which exceed those predicted for reflected light (Figs. 1, 3, and 4), and by similar near infrared energy distributions (Fig. 2), independent of T_{star} .

Both the $3.3 \mu\text{m}$ feature-to-continuum ratio, and the difference between K and the magnitude at $3.3 \mu\text{m}$, show a similar range of values for all the sources in which the $3.3 \mu\text{m}$ feature was detected. This is illustrated in Figure 5, which shows these two quantities plotted vs. T_{star} . All nebular positions with measurements at these wavelengths are shown.

The $3.3 \mu\text{m}$ feature-to-continuum ratio was derived by interpolating a continuum between the K and L' continuum measurements, and so is not calculated for nebulae for which there is no L' detection.

Figure 5 shows that while the $3.3 \mu\text{m}$ feature-to-continuum ratio has a similar range of values for all sources in which the feature was detected, there is also a significant scatter in this ratio, larger than the observational uncertainties. The $3.3 \mu\text{m}$ feature-to-continuum ratio varies from ~ 3 to ~ 9 , with a median of 5.3 and an average of 5.7.

It is possible that some of the variation in the $3.3 \mu\text{m}$ feature-to-continuum ratio is due to the K emission being due to a mixture of tiny particle emission and some other mechanism such as scattered starlight or molecular hydrogen emission. This would cause the continuum at $3.3 \mu\text{m}$ to be overestimated, when interpolating between K and L' , and thus the $3.3 \mu\text{m}$ feature-to-continuum ratio to be underestimated. To investigate this further, we have plotted in Figure 6 the $3.3 \mu\text{m}$ feature-to-continuum ratio vs. $K - L'$. All nebular positions with measurements at these wavelengths are shown. If the variation in the $3.3 \mu\text{m}$ feature-to-continuum ratio is due to contamination of the K emission by processes other than the tiny particle emission which dominates the L' emission, then we would expect higher values of the $3.3 \mu\text{m}$ feature-to-continuum ratio for larger values of $K - L'$. No such trend is seen in Figure 6; there is no correlation observed between the $3.3 \mu\text{m}$ feature-to-continuum ratio and $K - L'$.

Another possible explanation is that the material which emits the $3.3 \mu\text{m}$ feature is not identical to the material which emits the $3 \mu\text{m}$ continuum. One example of this is the $3.3 \mu\text{m}$ feature and the underlying continuum being due to different ranges of a size distribution of aromatic particles, but both groups of particles being excited by similar photon energies. For instance, the feature might be due to vibrational fluorescence of PAH molecules, and the continuum due to electronic fluorescence of amorphous carbon grains or PAH clusters. In this case, we would expect to see generally similar values of the $3.3 \mu\text{m}$ feature-to-continuum ratio in regions of tiny particle emission, as the particle size distribution is expected to be similar throughout the interstellar medium, but significant variations in the ratio could be caused by slight modifications of the particle size distribution by local conditions. Such variations in the $3.3 \mu\text{m}$ feature-to-continuum ratio might be uncorrelated with any changes in the mean photon energy (T_{star}) or shape of the continuum emission ($K - L'$), as is seen in Figures 5 and 6. The lack of correlation between $3.3 \mu\text{m}$ feature-to-continuum ratio and T_{star} (Fig. 5), however, suggests that the observed variation in the $3.3 \mu\text{m}$ feature-to-continuum ratio is not due simply to differences in the required excitation energy between the feature and its underlying continuum.

4.5. The effect of the temperature of the illuminating star

One goal of the observations presented in this paper was to test the proposals that the near infrared continuum emission and $3.3 \mu\text{m}$ emission was due to thermal emission from tiny grains stochastically heated by individual UV photons, as proposed in Papers I and II, or due to vibrational or electronic fluorescence from PAHs excited by UV radiation, as proposed by Léger & Puget (1984) and Allamandola, Tielens, & Barker (1985). The original three visual reflection nebulae whose observations are presented in Papers I and II had central stars with $T_{\text{star}} = 18,000\text{--}22,000$ K. Since the fraction of stellar luminosity available as UV photons is a strong function of spectral type, we hoped by extending the sample of visual reflection nebulae to hotter and cooler illuminating stars that we would be able to test the UV excitation hypothesis directly.

In Paper III IRAS surface photometry of visual reflection nebulae was used to study how the tiny grain or PAH emission depends on T_{star} . The ratio of surface brightness at $12 \mu\text{m}$ to the surface brightness at $100 \mu\text{m}$, I_{12}/I_{100} , was used as a measure of the relative amount of stellar energy absorbed and re-radiated by tiny grains and/or PAHs (at $12 \mu\text{m}$) and by large grains in equilibrium with the stellar radiation field (at $100 \mu\text{m}$). It was found that I_{12}/I_{100} is independent of T_{star} for $5,000 \text{ K} < T_{\text{star}} < 33,000 \text{ K}$. This is inconsistent with excitation of the $12 \mu\text{m}$ emission by UV radiation alone, but is consistent with the $12 \mu\text{m}$ emission being excited by photons with wavelengths ranging from 0.1 to $0.7 \mu\text{m}$. Because PAHs absorb most strongly at wavelengths $< 0.4 \mu\text{m}$ (Crawford, Tielens, & Allamandola 1985; Léger et al. 1989; Allamandola, Tielens, & Barker 1989), the results of Paper III suggest that the $12 \mu\text{m}$ IRAS emission is not due solely to free-flying PAH molecules.

The observation that I_{12}/I_{100} is independent of T_{star} (Paper III) does not rule out some contribution by PAH molecules to the $12 \mu\text{m}$ emission, but does show that there must be at least one component to the $12 \mu\text{m}$ emission that absorbs over a wider range of UV and visual wavelengths than the narrow range of wavelengths at which PAHs absorb. The IRAS $12 \mu\text{m}$ band covers $8.0 - 14.9 \mu\text{m}$ (FWHM, from IRAS Explanatory Supplement) and so can include emission from several components: strong emission features at 7.7 , 8.6 , and $11.3 \mu\text{m}$; a weaker emission feature at $12.7 \mu\text{m}$; a plateau of emission at $11\text{--}13 \mu\text{m}$; and continuum emission throughout the filter (see Allamandola, Tielens, & Barker 1989 for a review). Roche, Aitken, & Smith (1989) and Bregman et al. (1989) observe that the $11.3 \mu\text{m}$ emission has a different spatial distribution in the Orion Bar than the nearby continuum emission, indicating these arise from distinct components of the interstellar medium. Bregman et al. (1994) find that images at 3.3 , 8.4 , and $11.3 \mu\text{m}$ of the Orion Bar all look different, again supporting the idea that different components are responsible for emission in different features. Allamandola, Tielens, & Barker (1989) have identified emission from

PAHs, PAH clusters, and amorphous carbon grains as contributing to different emission components seen in the IRAS 12 μm band. Thus the results of Paper III could be consistent with PAH molecular emission contributing to the 12 μm IRAS emission, as long as there is also one or more other materials, such as PAH clusters or amorphous carbon grains, which are able to absorb over a wide wavelength range in the visible and UV and emit within the 12 μm IRAS band.

If the extended near infrared emission, in excess of reflected light, is due to some sort of non-equilibrium thermal emission from tiny grains (Paper II), then it would be interesting to search for temperature differences between nebulae with different values of T_{star} . The best indicator of tiny grain temperature should be $K - L'$, because the excess infrared emission is stronger, relative to any reflected light component, at longer wavelengths (Sellgren et al. 1985; Papers III and IV). If instead the emission is due to UV fluorescence from PAHs (Léger and Puget 1984; Allamandola et al. 1985) then $K - L'$ is an indicator of whether the emitted fluorescent spectrum changes with excitation. Figure 7 shows $J - H$, $H - K$, and $K - L'$ plotted vs. T_{star} . All nebular positions with measurements at these wavelengths are shown. There is no evidence for changing $J - H$, $H - K$, or $K - L'$ color with T_{star} . The nebular offsets for the near infrared data ($\sim 42''$) and the IRAS data from Paper III ($\sim 180''$) were too different for a comparison of the near and mid infrared data.

We do not see any dependence on T_{star} for either the 3.3 μm feature-to-continuum ratio or the $K - L'$ color among the stars for which we have such observations (Figs. 5 and 7), over a factor of two range in T_{star} . In Paper III we found that the nebulae illuminated by the coolest stars in our sample provided the necessary range in T_{star} to rule out the IRAS 12 μm emission being due purely to PAH molecules. We would have liked to extend our observations of the 3.3 μm feature-to-continuum ratio or the $K - L'$ color to even lower values of T_{star} , but we found that the visual reflection nebulae with higher K surface brightnesses were largely confined to the hottest illuminating stars in our sample. We did not have enough sensitivity to obtain near infrared colors and 3.3 μm spectrophotometry in visual reflection nebulae with K surface brightnesses below 0.3 MJy sr^{-1} . Thus our observations currently do not have enough range in T_{star} to confirm or rule out models in which the near infrared continuum emission or 3.3 μm emission is due to PAH molecules. This test must await more sensitive observations, such as may be possible from ISO, SIRTF, or IRTS.

5. Summary

We have extended the observations of Papers I and II, to a survey of near infrared emission in a total of 23 visual reflection nebulae. Extended near infrared continuum emission at 1–5 μm and emission from a spectral feature at 3.3 μm in the three visual reflection nebulae studied in Papers I and II has been attributed to either thermal emission from stochastically heated tiny grains (Papers I and II) or to vibrational or electronic fluorescence from polycyclic aromatic hydrocarbon (PAH) molecules (Léger & Puget 1984; Allamandola, Tielens, & Barker 1985, 1989). Our new observations report on a search for extended 2.2 μm emission in visual reflection nebulae illuminated by stars with spectral types ranging from O9.5V to M1IIIe.

We have detected extended 2.2 μm emission, after correction for instrumental scattered light, in 16 out of 23 nebulae studied, illuminated by stars with spectral types ranging from O9.5V to F5Iab. For most of these 16 nebulae we have measured $J - K$, $H - K$, and $K - L'$, as well as obtaining surface brightness measurements at the wavelength of the 3.3 μm emission feature. We use several approaches to predict the K surface brightness of scattered starlight in these nebulae, in order to determine whether our K surface brightnesses are consistent with, or in excess over, scattered starlight. The only source which has near infrared colors and a K surface brightness consistent with being due primarily to scattered starlight is NGC 1999; the remaining sources with extended K emission are all consistent with some or all of their infrared emission being due to tiny grains and/or PAHs.

All of the reflection nebulae with extended near infrared emission in excess over scattered starlight have very similar near infrared colors and show the 3.3 μm feature in emission with similar feature-to-continuum ratios. The three reflection nebulae previously studied in Papers I and II, while having high surface brightnesses, are still very representative of our larger sample. The 3.3 μm feature-to-continuum ratio ranges from ~ 3 to ~ 9 , both within individual nebulae and from nebula to nebula; this variation does not appear to depend on T_{star} or $K - L'$. One possible explanation for this is that the 3.3 μm feature and its underlying continuum arise from different materials, or from different ranges of sizes within a size distribution of particles. No dependence on T_{star} is seen in the near infrared colors or 3.3 μm feature-to-continuum ratio, over a factor of two range in T_{star} . We do not have the sensitivity at present to obtain a wider range in T_{star} , to test whether or not this is in conflict with models of tiny grain or PAH emission. ISO, SIRTF, or IRTS may be able to make these tests with higher sensitivity in future.

We would like to thank the IRTF and UKIRT staffs for their superb technical support. We also thank Tom Geballe, Bill Golisch, Dave Griep, Bob Howell, Charlie Kaminski,

Martina McGinn, Mark Shure, Xander Tielens, Alan Tokunaga, and Doug Toomey for assistance with the observations. We are grateful to Darren DePoy, Jay Frogel, and Doug Whittet for suggestions on improving our paper. This work was carried out in part at the Jet Propulsion Laboratory, California Institute of Technology, under contract with the National Aeronautics and Space Administration. This research has made use of the Simbad database, operated at CDS, Strasbourg, France.

TABLE 1

Characteristics of Nebular Illuminating Stars

vdB No. ^a	Nebula Name	Star Name	V	$E(B - V)$	Spectral Type	T_{star} (K) ^c	Ref. ^d
10	...	HD 20041	5.81	0.71	A0Ia	9,400	1
16	...	BD+29 565	9.16	0.30	F0V	7,000	1
17	NGC 1333	BD+30 549	10.47	0.60	B8V	11,000	1
22	Merope Nebula ^b	23 Tau ^b	4.18	0.09	B6IVnn	12,000	1
...	IC 359	Elias 1 ^b	16.2	1.3 ^e	A6e	8,100	2, 3
34	...	AE Aur ^b	5.97	0.53	O9.5V	33,000	1
35	...	HD 34033	8.66	0.13	G8II–III	4,900	1
46	NGC 1999	V380 Ori ^b	10.22	0.70	A0–2e	9,500	1, 4
52	NGC 2023	HD 37903	7.82	0.36	B1.5V	22,000	1
57	IC 435	HD 38087	8.30	0.35	B3n	18,000	1
59	NGC 2068	HD 38563N	10.56	1.42	B2II–III	19,000	5
60	NGC 2071	HD 290861a	10.14	1.25	B2–3	19,000	5
72	...	HD 42261	9.18	0.41	B3V	18,000	1
74	...	BD–6 1444	10.82	0.63	B6	13,000	1
...	Parsamyan 18 ^b	star A	13.21	1.26	B2–3e	19,000	6
101	...	HD 146834	6.35	0.33	G5III	5,000	1
111	...	HD 156697	6.50	0.11 ^f	F0n	7,000	1
133	...	HD 195593	6.19	0.65	F5Iab	6,800	1
135	...	BD+31 4152	8.43	0.40	M1IIIe	3,600	1
137	IC 5076	HD 199478	5.69	0.50	B8Ia	10,000	1
139	NGC 7023	HD 200775	7.39	0.44	B3e	18,000	1, 7
146	NGC 7129	BD+65 1637	10.15	0.67	B2nne	21,000	1
152	Ced 201	BD+69 1231	9.29	0.21	B9.5V	10,000	1

(a) Number in reflection nebula catalog of van den Bergh (1966).

(b) Other designations: Merope nebula = NGC 1435; 23 Tau = HD 23480; Elias 1 = V892 Tau; AE Aur = HD 34078; V380 Ori = BD–6 1253; Parsamyan 18 = NGC 2316.

(c) Temperature of central star, T_{star} , derived from spectral type using calibrations of Panagia (1973) for B3 and earlier stars and Johnson (1966) for the remaining stars.

(*d*) References—(1) Racine 1968; (2) Elias 1978; (3) Cohen & Kuhi 1979; (4) Herbig 1960; (5) Strom et al. 1975; (6) see note (*g*) to this Table; (7) Witt & Cottrell 1980*b*.

(*e*) $E(B - V)$ for Elias 1 derived from $B - V = 1.5$ (Elias 1978) and adopting $(B - V)_0 = 0.17$ for A6V (Johnson 1966).

(*f*) $E(B - V)$ for HD 156697 derived from $B - V = 0.41$ (Racine 1968) and adopting $(B - V)_0 = 0.31$ for F0V (Johnson 1966).

(*g*) Parsamyan 18 contains a B2–3 star which excites a compact H II region (López et al. 1988). López et al. (1988) suggest that the two condensations visible in Parsamyan 18 are not stars but rather knots of nebulosity due to light reflected from an obscured H II region. These two condensations, however, have stellar spectra and are not identical; the northeast component, star A, is a B emission line star, and the southwest component is an A–F star (Humphreys 1985; Strom 1985). It seems reasonable to identify star A with the exciting star of the H II region, giving a spectral type of B2–3e. Star A has $V = 13.21$ and $B - V = 1.04$ (Humphreys 1985), which was combined with an assumed $(B - V)_0 = -0.22$ for B2.5V (Johnson 1966) to derive $E(B - V)$.

TABLE 2

Chopper Throws Used

Name	Chopper Throws
vdB 10	180" EW
vdB 16	180" EW
vdB 17	120" EW, 180" NS
vdB 22	180" EW, 180" NS, 342" EW, 377" EW
Elias 1	180" EW, 180" NS
vdB 34	120" EW, 180" EW
vdB 35	180" EW
vdB 46	180" EW
vdB 52	210" EW, 250" EW
vdB 57	180" EW, 180" NS
vdB 59	180" EW, 210" EW
vdb 60	180" EW, 180" NS
vdb 72	180" EW
vdb 74	180" EW
Parsamyan 18	120" EW, 180" EW
vdb 101	180" EW
vdb 111	180" EW
vdb 133	120" EW, 180" EW, 180" NS
vdb 135	180" EW
vdb 137	120" EW, 180" EW
vdb 139	120" EW, 150" EW, I 160" EW
vdb 146	180" EW, 180" NS
vdb 152	180" NS

TABLE 3a

2.2 μm Surface Brightness of Reflection Nebulae

S_ν (MJy sr $^{-1}$) at Given Nebular Offset^b

Name	Ap ^a	30"E 30"N	30"E 30"S	30"W 30"N	30"W 30"S
vdB 10	6.2"	2.02 ± 0.12	...
	7.7"	2.15 ± 0.27	...	1.73 ± 0.20	< 0.42
	10.5"	0.23 ± 0.07	...	1.64 ± 0.12	...
vdB 16	10.5"	< 0.16	< 0.10	< 0.12	< 0.08
vdB 17	8.2"	< 1.36	3.26 ± 0.87	...	< 2.89
vdB 22	10.5"	< 2.75	< 0.27	< 0.37	0.31 ± 0.05
	19.6"	0.35 ± 0.09
Elias 1	6.2"	< 0.69
	10.5"	< 0.68	...	< 0.08	< 0.13
vdB 34	6.2"	...	0.27 ± 0.05
	10.5"	0.47 ± 0.06	0.51 ± 0.05	< 0.55	...
	19.6"	...	0.34 ± 0.04
vdB 35	10.5"	< 0.51	< 0.06	< 0.10	< 0.11
vdB 46	6.2"	0.45 ± 0.13	...
	10.5"	< 0.46	0.29 ± 0.03	0.45 ± 0.05	0.21 ± 0.04

TABLE 3a, Continued

2.2 μm Surface Brightness of Reflection Nebulae

S_ν (MJy sr $^{-1}$) at Given Nebular Offset^b

Name	Ap ^a	30"E 30"N	30"E 30"S	30"W 30"N	30"W 30"S
vdB 57	6.2"	...	0.33 ± 0.07
	10.5"	...	0.43 ± 0.05
vdB 60	6.2"	...	6.14 ± 0.35
	10.5"	5.09 ± 0.34	5.52 ± 0.31	1.41 ± 0.08	5.13 ± 0.29
vdB 72	6.2"	1.84 ± 0.14
	10.5"	1.78
vdB 74	6.2"	0.67 ± 0.08
	10.5"	0.57 ± 0.05	0.54 ± 0.09	...	0.47 ± 0.09
	19.6"	0.47 ± 0.07
vdB 101	7.7"	< 0.32	< 0.15	< 0.13	< 0.18
vdB 111	6.2"	...	0.22 ± 0.03
	7.7"	...	0.22 ± 0.02	...	< 0.03

TABLE 3a, Continued

2.2 μm Surface Brightness of Reflection Nebulae

Name	Ap ^a	S_ν (MJy sr ⁻¹) at Given Nebular Offset ^b					
		30''E 30''N	30''E 30''S	30''W 30''N	30''W 30''S	30''W 30''S	30''W 30''S
vdB 133	6.2''	< 4.71	
	8.2''	< 2.49	< 3.21	< 3.36	< 3.10		
	10.5''	2.14	< 0.24	< 0.28	< 0.25		
	19.6''	2.82 ± 0.35		
vdB 135	7.7''	< 0.37	< 0.16	...	0.65 ± 0.09		
vdB 137	6.2''	< 0.28		
	10.5''	< 0.12	...	< 0.14	0.39 ± 0.09		
vdB 146	6.2''	1.36 ± 0.13		
	8.2''	< 2.66	3.14 ± 0.60	...	< 1.41		
	9.2''	0.92		
vdB 152	10.5''	1.14 ± 0.09	5.24 ± 0.32	2.08 ± 0.12	...		
	8.2''	< 1.96	< 2.15	< 1.47	< 0.79		

TABLE 3b

2.2 μm Surface Brightness of Reflection Nebulae

Name	Ap ^a	Nebular Offset ^b		S_ν (2.2 μm)	
		$\Delta\alpha$	$\Delta\delta$	(MJy sr ⁻¹)	
vdB 17	6.2''	0''E	20''S	1.12	± 0.14
	8.2''	30''W	0''N	< 2.72	
	8.2''	30''E	0''N	< 3.94	
	10.5''	0''E	20''S	1.24	± 0.07
vdB 22	8.2''	30''W	0''N	< 2.73	
	8.2''	30''E	0''N	< 3.24	
	10.5''	0''E	557''S	< 0.27	
	10.5''	0''E	135''S	< 0.09	
	10.5''	0''E	125''S	0.09	± 0.03
Elias 1	8.2''	30''W	0''N	< 3.12	
	8.2''	30''E	0''N	< 4.31	
vdB 52	10.5''	40''W	40''S	5.23	± 0.73
	10.5''	0''E	60''S	6.59	± 0.91
	10.5''	0''E	60''N	2.81	± 0.32
vdB 59	10.5''	60''E	40''S	1.57	± 0.09
vdB 60	8.2''	30''E	0''N	4.47	± 1.03
Parsamyan 18	6.2''	12''W	0''N	7.13	± 0.92
	6.2''	12''W	12''N	3.28	± 0.35
	6.2''	0''E	12''S	7.46	± 0.81
	6.2''	0''E	12''N	6.04	± 0.67
	6.2''	12''E	0''N	2.19	± 0.36
	10.5''	15''W	0''N	5.44	± 0.34
	10.5''	12''W	12''N	3.79	
vdB 133	6.2''	20''E	30''N	< 4.70	
	6.2''	30''E	20''N	< 4.68	
	8.2''	30''W	0''N	< 4.51	
	8.2''	30''E	0''N	< 3.95	
	10.5''	20''E	30''N	1.82	± 0.42
	10.5''	30''E	20''N	1.07	± 0.32

TABLE 3b, Continued

2.2 μm Surface Brightness of Reflection Nebulae

Name	Ap ^a	Nebular Offset ^b		S_ν (2.2 μm) (MJy sr ⁻¹)	
		$\Delta\alpha$	$\Delta\delta$		
vdB 139	6.2''	52''W	34''N	3.89	
	6.2''	44''W	27''N	7.58	
	6.2''	35''W	20''N	8.36	
	6.2''	30''W	20''N	7.19	
	6.2''	0''E	30''N	5.90	± 0.34
	10.5''	30''W	20''N	9.19	
	10.5''	0''E	60''S	1.89	± 0.40
	10.5''	0''E	30''N	7.37	± 0.41
	10.5''	0''E	60''N	2.70	± 0.56
	10.5''	0''E	120''N	0.35	± 0.10
vdB 146	8.2''	30''W	0''N	< 2.44	
	8.2''	30''E	0''N	5.25	± 0.86
vdB 152	8.2''	30''W	0''N	< 0.75	
	8.2''	30''E	0''N	< 1.42	

(a) Aperture diameter in arcseconds.

(b) Offset from central star of nebular position, in arcseconds.

Note to Table—Uncertainties are $\pm 1\text{-}\sigma$. Upper limits are $3\text{-}\sigma$.

TABLE 4

Infrared Colors of Reflection Nebulae

Name	Ap ^a	Nebular Offset ^b		$J - K$	$J - H$	$H - K$	$K - [3.3 \mu\text{m}]$	$K - L'$
		$\Delta\alpha$	$\Delta\delta$					
vdB 10	10.5''	30''W	30''N	0.70 ± 0.12	0.41 ± 0.12	0.29 ± 0.11	< 1.67	< 0.42
vdB 17	6.2''	0''E	20''S	1.72 ± 0.22	0.71 ± 0.23	1.01 ± 0.20	4.39 ± 0.30	3.39 ± 0.32
	8.2''	30''E	30''S	> 0.81
	10.5''	0''E	20''S	1.72 ± 0.11	0.88 ± 0.12	0.83 ± 0.10	4.46 ± 0.11	2.56 ± 0.16
vdB 22	10.5''	30''W	30''S	> 0.87	...	> 0.78	< 4.21	2.93 ± 0.29
	10.5''	0''E	125''S	> -0.29	...	> 0.36
	19.6''	30''W	30''S	< 2.28	< 1.77
vdB 34	10.5''	30''E	30''S	0.22 ± 0.13	0.30 ± 0.14	-0.09 ± 0.16	< 3.02	< 2.09
	19.6''	30''E	30''S	< 3.23	< 2.56
vdB 46	10.5''	30''W	30''N	0.38 ± 0.17	0.35 ± 0.19	0.03 ± 0.19
vdB 52	10.5''	40''W	40''S	1.83 ± 0.19	0.94 ± 0.16	0.89 ± 0.19	...	2.39 ± 0.21
	10.5''	0''E	60''S	2.13 ± 0.19	1.25 ± 0.16	0.88 ± 0.19	3.87 ± 0.21	2.30 ± 0.21
	10.5''	0''E	60''N	1.95 ± 0.20	0.88 ± 0.21	1.07 ± 0.18	3.03 ± 0.26	1.94 ± 0.27
vdB 57	10.5''	30''E	30''S	1.91 ± 0.18	0.89 ± 0.17	1.02 ± 0.16	3.68 ± 0.26	< 2.10

TABLE 4, Continued

Infrared Colors of Reflection Nebulae

Name	Nebular Offset ^b			$J - K$	$J - H$	$H - K$	$K - [3.3 \mu\text{m}]$	$K - L'$
	Ap ^a	$\Delta\alpha$	$\Delta\delta$					
vdB 59	10.5''	60''E	40''S	1.78	0.71	1.06	3.76	2.38
				± 0.24	± 0.31	± 0.22	± 0.25	± 0.30
vdB 60	10.5''	30''E	30''S	2.54	1.15	1.39	3.24	2.49
				± 0.10	± 0.11	± 0.09	± 0.13	± 0.13
vdB 72	10.5''	30''W	30''S	2.07	1.18	0.89	3.61	2.45
				± 0.12	± 0.11	± 0.08	± 0.20	± 0.15
vdB 74	10.5''	30''E	30''N	1.77	1.01	0.76	< 3.40	< 1.91
				± 0.27	± 0.33	± 0.23		
	19.6''	30''E	30''N	1.79	...
							± 0.37	
Parsamyan 18	6.2''	12''W	0''N	4.22	2.78
							± 0.21	± 0.29
	6.2''	12''W	12''N	4.39	2.82
							± 0.19	± 0.30
	6.2''	0''E	12''S	3.20	1.98
							± 0.20	± 0.28
	6.2''	0''E	12''N	4.42	2.70
							± 0.19	± 0.28
	6.2''	12''E	0''N	3.99	2.97
							± 0.27	± 0.33
	10.5''	15''W	0''N	4.12	2.98
							± 0.13	± 0.10
	10.5''	12''W	12''N	1.88	0.97	0.91	4.48	2.78
				± 0.09	± 0.10	± 0.07	± 0.13	± 0.19
vdB 133	10.5''	20''E	30''N	1.16	0.82	0.34	...	< 0.98
				± 0.39	± 0.39	± 0.36		
	10.5''	30''E	30''N	0.89
								± 0.31
	19.6''	30''E	30''N	< 1.38	...

TABLE 4, Continued

Infrared Colors of Reflection Nebulae

Name	Ap ^a	Nebular Offset ^b		$J - K$	$J - H$	$H - K$	$K - [3.3 \mu\text{m}]$	$K - L'$
		$\Delta\alpha$	$\Delta\delta$					
vdB 139	6.2''	52''W	34''N	3.74	2.01
							± 0.13	± 0.11
	6.2''	44''W	27''N	4.47	2.63
							± 0.08	± 0.08
	6.2''	35''W	20''N	3.83	2.58
							± 0.09	± 0.07
	10.5''	30''W	20''N	2.04	1.11	0.93	3.69	2.24
				± 0.07	± 0.12	± 0.12	± 0.16	± 0.08
	10.5''	0''E	60''S	4.03	2.55
						± 0.32	± 0.35	
10.5''	0''E	30''N	2.10	1.08	1.02	3.60	2.31	
			± 0.10	± 0.10	± 0.09	± 0.22	± 0.10	
10.5''	0''E	60''N	3.89	2.20	
						± 0.32	± 0.33	
10.5''	0''E	120''N	< 4.92	< 3.80	
vdB 146	6.2''	30''E	30''N	1.10	0.60	0.50	...	2.72
				± 0.16	± 0.17	± 0.14		± 0.27
	9.2''	30''E	30''N	4.38	3.44
						± 0.20	± 0.21	

(a) Aperture diameter in arcseconds.

(b) Offset from central star of nebular position, in arcseconds.

Note to Table—Uncertainties are $\pm 1\text{-}\sigma$. Upper and lower limits are $3\text{-}\sigma$.

TABLE 5

Infrared Magnitudes of Illuminating Stars of Reflection Nebulae

Name	Ap ^a	<i>J</i>	<i>H</i>	<i>K</i>	[3.3 μm]	<i>L'</i>
vdB 10	7.7''	3.75
				± 0.10		
	10.5''	...	3.96	3.85	3.65	3.46
					± 0.16	± 0.10
vdB 16	10.5''	7.64
				± 0.06		
vdB 17	6.2''	8.81	8.49	8.30	8.06	8.06
		± 0.15	± 0.11	± 0.11	± 0.14	± 0.24
	8.2''	8.87	8.52	8.30
		± 0.07	± 0.13	± 0.18		
	10.5''	8.84	8.49	8.31	7.82	8.10
		± 0.06				
vdB 22	8.2''	4.17
				± 0.18		
	10.5''	4.28	4.29	4.26
					± 0.09	
	19.6''	4.32	4.32	4.49
				± 0.10	± 0.21	± 0.20
	57.0''	4.29	4.24	4.24
Elias 1	8.2''	5.60
				± 0.18		
	10.5''	8.78	6.95	5.80	4.72	4.41
		± 0.07		± 0.06	± 0.10	± 0.10
vdB 34	6.2''	5.32	5.31	5.27	5.25	5.22
		± 0.15	± 0.11	± 0.11	± 0.14	± 0.24
	19.6''	5.23	5.34	5.49
				± 0.10	± 0.21	± 0.20
vdB 35	10.5''	6.12
				± 0.19		

TABLE 5, Continued

Infrared Magnitudes of Illuminating Stars of Reflection Nebulae

Name	Ap ^a	<i>J</i>	<i>H</i>	<i>K</i>	[3.3 μ m]	<i>L'</i>
vdB 46	10.5''	8.19 \pm 0.07	7.07	6.20 \pm 0.06
vdB 52	6.2''	7.37 \pm 0.15	...	7.01 \pm 0.11
	10.5''	7.55 \pm 0.11	7.45 \pm 0.11	7.38 \pm 0.12	6.85 \pm 0.21	7.10 \pm 0.10
vdB 57	10.5''	7.64	7.37	7.25	7.32	7.21
vdB 59	10.5''	7.64 \pm 0.21	7.13 \pm 0.21	6.82 \pm 0.21	6.63 \pm 0.21	6.73 \pm 0.21
vdB 60	8.2''	7.05 \pm 0.07	...	6.81 \pm 0.19
	10.5''	7.11 \pm 0.07	6.60	6.42 \pm 0.06	6.27 \pm 0.10	6.16 \pm 0.10
vdB 72	6.2''	8.65
	10.5''	8.71	8.63	8.59	...	8.31 \pm 0.07
vdB 74	10.5''	9.70 \pm 0.18	9.48 \pm 0.18	9.25 \pm 0.06	8.23 \pm 0.10	8.43 \pm 0.10
Parsamyan 18	6.2''	10.32 \pm 0.15	9.68 \pm 0.11	9.19 \pm 0.11	7.46 \pm 0.14	7.92 \pm 0.24
	10.5''	6.74 \pm 0.23	...
vdB 101	7.7''	3.67 \pm 0.10
vdB 111	7.7''	5.60

TABLE 5, Continued

Infrared Magnitudes of Illuminating Stars of Reflection Nebulae

Name	Ap ^a	<i>J</i>	<i>H</i>	<i>K</i>	[3.3 μm]	<i>L'</i>
vdB 133	6.2''	3.12 ± 0.13
	8.2''	4.24 ± 0.10	3.78 ± 0.13	3.58 ± 0.18
	10.5''	3.44 ± 0.08
	19.6''	3.56 ± 0.21	...
vdB 135	7.7''	3.57 ± 0.10
vdB 137	10.5''	...	4.45	4.35
vdB 139	6.2''	4.76	...	3.36
	10.5''	6.09	5.41	4.63	3.58 ± 0.21	3.37
vdB 146	6.2''	8.48	...	8.00 ± 0.06
	8.2''	8.34 ± 0.11
	9.2''	8.44	8.02 ± 0.12	8.21 ± 0.09
	10.5''	8.83 ± 0.07	8.57	8.36 ± 0.06
vdB 152	8.2''	8.93 ± 0.07	8.85 ± 0.13	9.04 ± 0.11

(a) Aperture diameter in arcseconds.

Note to Table—Uncertainties are $\pm 1\text{-}\sigma$, and are only given when larger than 0.05 mag.

TABLE 6
10 and 20 Micron Magnitudes of
Illuminating Stars of Reflection Nebulae

Nebula	N	Q
vdB 9	4.10 ± 0.10	...
vdB 10	3.63 ± 0.08	...
vdB 12	3.53	3.35 ± 0.09
vdB 16	7.64 ± 0.15	...
17 Tau	3.77	3.72 ± 0.14
20 Tau	3.99 ± 0.09	...
23 Tau	3.92 ± 0.08	3.70 ± 0.19
25 Tau	2.43	2.04 ± 0.08
vdB 25	4.47	>4.46
AE Aur	5.37 ± 0.11	...
vdB 35	5.98 ± 0.07	...
vdB 37	0.84	0.69
vdB 40	5.78 ± 0.08	...
vdB 41	8.13 ± 0.34	...
vdB 47	2.68 ± 0.08	2.66 ± 0.08
NGC 2068	5.66 ± 0.10	...
NGC 2071	6.51 ± 0.24	...
vdB 61	5.59 ± 0.10	...
vdB 62	6.40 ± 0.12	...
vdB 133	3.46 ± 0.10	3.50 ± 0.26
vdB 136	3.13 ± 0.10	2.88 ± 0.24
vdB 135	3.39 ± 0.10	3.53 ± 0.28
vdB 137	4.07 ± 0.10	...

Note to Table—Uncertainties are $\pm 1\text{-}\sigma$, and are only given when larger than 0.05 mag. Lower limits are $3\text{-}\sigma$. Aperture diameter was $6''$ for all measurements.

TABLE 7

Estimated 2.2 μm Nebular Optical Depths

Nebula	$\tau(K)^a$	$\tau(K)^b$
10	...	0.0027
17	0.098 – 0.155	0.108
22	0.0066 – 0.0843	0.0140
34	...	0.00051
35	...	0.030
46	0.18 – 0.57	...
52	0.083 – 0.123	0.108
57	0.0170	0.0073
59	1.32 – 2.48	0.11
60	0.060 – 0.275	0.108
72	0.068	0.108
74	0.021 – 0.038	0.108
9918	0.16 – 1.08	0.11
101	...	0.0067
111	...	0.0075
133	...	0.0080
135	...	0.028
137	0.00095	...
139	0.045 – 0.093	0.055
146	0.066 – 0.166	...
152	0.014 – 0.079	...

Notes to Table:

(a) Nebular optical depth at K , $\tau(K)$, derived from Equation 3 combined with visual observations of reflected light (Racine 1971; Witt 1977; Witt & Cottrell 1980a; Cottrell 1981; Witt, Schild, & Kraiman 1984; Witt 1985b, 1986; Witt & Schild 1986; Witt et al. 1987) to estimate the visual optical depth, $\tau(V)$, for each nebula, with $\tau(K) = \tau(V) / 9.29$ (Mathis 1990).

(b) Nebular optical depth at K , $\tau(K)$, derived from the value of $A_V(neb)$ calculated in Paper III, which is an estimate of $\tau(V)$ for each nebula calculated from the amount of starlight incident on the nebula which is reradiated in the far infrared, with $\tau(K) = \tau(V) / 9.29$ (Mathis 1990).

REFERENCES

- Aitken, D. K. 1981, in *IAU Symposium 96, Infrared Astronomy*, ed. C. G. Wynn-Williams & D. P. Cruikshank (Dordrecht: Reidel), p. 207
- Allamandola, L. J., Tielens, A. G. G. M., & Barker, J. R. 1985, *ApJ*, 290, L25
- Allamandola, L. J., Tielens, A. G. G. M., & Barker, J. R. 1989, *ApJS*, 71, 733
- Allen, D. A., Baines, D. W. T., Blades, J. C., & Whittet, D. C. B. 1982, *MNRAS*, 199, 1017
- Balm, S. P., & Kroto, H. W. 1990, *MNRAS*, 245, 193
- Becklin, E. E. and Neugebauer, G. 1968, *ApJ*, 151, 145
- Blanco, A., Bussoletti, E., & Colangeli, L. 1988, *ApJ*, 334, 875
- Borghesi, A., Bussoletti, E., & Colangeli, L. 1987, *ApJ*, 312, 422
- Bregman, J. D. 1989, in *IAU Symposium 135, Interstellar Dust*, ed. L. J. Allamandola & A. G. G. M. Tielens (Dordrecht: Kluwer), p. 109
- Bregman, J. D., Allamandola, L. J., Tielens, A. G. G. M., Geballe, T. R., & Witteborn, F. C. 1989, *ApJ*, 344, 791
- Bregman, J., Larson, K., Rank, D., & Temi, P. 1994, *ApJ*, 423, 326
- Brooke, T. Y., Tokunaga, A. T., & Strom, S. E. 1993, *AJ*, 106, 656
- Castelaz, M. W., Sellgren, K., & Werner, M. W. 1987, *ApJ*, 313, 853
- Cohen, M. & Kuhl, L. V. 1979, *ApJS*, 41, 743
- Cohen, M., Tielens, A. G. G. M., & Allamandola, L. J. 1985, *ApJ*, 299, L93
- Cohen, M. et al. 1986, *ApJ*, 302, 737
- Cohen, M., Walker, R. G., Barlow, M. J., & Deacon, J. R. 1992, *AJ*, 104, 1650
- Cottrell, M. J. 1981, Ph.D. thesis, University of Toledo
- Crawford, M. K., Tielens, A. G. G. M., & Allamandola, L. J. 1985, *ApJ*, 293, L45
- Draine, B. T., & Lee, H. M. 1984, *ApJ*, 285, 89
- Duley, W. W. & Williams, D. A. 1981, *MNRAS*, 196, 269
- Elias, J. H., Frogel, J. A., Matthews, K., & Neugebauer, G. 1982, *AJ*, 87, 1029
- Elias, J. H. 1978, *ApJ*, 224, 857
- Henry, L. G., & Greenstein, J. L. 1941, *ApJ*, 93, 70

- Herbig, G. H. 1960, *ApJS*, 4, 337
- Humphreys, R. 1985, private communication
- Johnson, H. L. 1966, *ARAA*, 4, 193
- Jourdain de Muizon, M., d'Hendecourt, L. B., & Geballe, T. R. 1990, *A&A*, 227, 526
- Kim, S.-H., Martin, P. G., & Hendry, P. D. 1994, *ApJ*, 422, 164
- Léger, A., & Puget, J. L. 1984, *A&A*, 137, L5
- Léger, A., d'Hendecourt, L., & Défourneau, D. 1989, *A&A*, 216, 148
- López, J. A., Roth, M., Friedman, S. D., & Rodríguez, L. F. 1988, *Rev Mex Astron Ap*, 16, 99
- Mathis, J. S. 1990, *ARAA*, 28, 37
- Neugebauer, G., Oke, J. B., Becklin, E. E., & Matthews, K. 1979, *ApJ*, 230, 79
- Ogmen, M. & Duley, W. W. 1988, *ApJ*, 334, L117
- Panagia, N. 1973, *AJ*, 78, 929
- Papoular, R., Conard, J., Guiliano, M., Kister, J., & Mille, G. 1989, *A&A*, 217, 204
- Puget, J. L. & Léger, A. 1989, *ARA&A*, 27, 161
- Racine, R. 1968, *AJ*, 73, 233
- Racine, R. 1971, *AJ*, 76, 321
- Roche, P. F., Aitken, D. K., & Smith, C. H. 1989, *MNRAS*, 236, 485
- Roche, P. F., Aitken, D. K., & Smith, C. H. 1994, *MNRAS*, 269, 649
- Sakata, A., Wada, S., Onaka, T., and Tokunaga, A. T. 1987, *ApJ*, 320, L63
- Saperstein, D. D., Metin, S. S., & Kaufman, J. H. 1989 *ApJ*, 342, L47
- Schutte, W. A., Tielens, A. G. G. M., Allamandola, L. J., Cohen, M., & Wooden, D. H. 1990, *ApJ*, 360, 577
- Sellgren, K. 1983, Ph.D. thesis, California Inst. Technology
- Sellgren, K. 1984, *ApJ*, 277, 623 (Paper II)
- Sellgren, K., Werner, M. W., & Dinerstein, H. L. 1983, *ApJ*, 271, L13 (Paper I)
- Sellgren, K., Allamandola, L. J., Bregman, J. D., Werner, M. W., & Wooden, D. H. 1985, *ApJ*, 299, 416
- Sellgren, K., Luan, L., & Werner, M. W. 1990, *ApJ*, 359, 384 (Paper III)
- Sellgren, K., Werner, M. W., & Dinerstein, H. L. 1992, *ApJ*, 400, 238 (Paper IV)

- Strom, K. 1985, private communication, based on an unpublished spectrum by R. Humphreys
- Strom, K. M., Strom, S. E., Carrasco, L., & Vrba, F. J. 1975, *ApJ*, 196, 489
- Tokunaga, A. T. 1986, *IRTF Photometry Manual*
- Tokunaga, A. T., Sellgren, K., Smith, R. G., Nagata, T., Sakata, A., & Nakada, Y. 1991, *ApJ*, 380, 452
- van den Bergh, S. 1966, *AJ*, 71, 990
- Wdowiak, T. J., Flickinger, G. C., & Cronin, J. R. 1988, *ApJ*, 328, L75
- Webster, A. 1991, *Nature*, 352, 412
- Whittet, D. C. B., Williams, P. M., Bode, M. F., Davies, J. K. & Zealey, W. J. 1983, *A&A*, 123, 301
- Whittet, D. C. B., McFadzean, A. D., & Geballe, T. R. 1984, *MNRAS*, 211, 29P
- Willner, S. P. 1984, in *Galactic and Extragalactic Infrared Spectroscopy*, ed. M. F. Kessler & J. P. Phillips (Dordrecht: Reidel), p. 37
- Witt, A. N. 1977, *PASP*, 89, 750
- Witt, A. N. 1985*a*, *ApJ*, 294, 216
- Witt, A. N. 1985*b*, private communication
- Witt, A. N. 1986, private communication
- Witt, A. N., & Cottrell, M. J. 1980*a*, *AJ*, 85, 22
- Witt, A. N., & Cottrell, M. J. 1980*b*, *ApJ*, 235, 899
- Witt, A. N., Schild, R. E., & Kraiman, J. B. 1984, *ApJ*, 281, 708
- Witt, A. N. & Schild, R. E. 1985, *ApJ*, 294, 225
- Witt, A. N. & Schild, R. E. 1986, *ApJS*, 62, 839
- Witt, A. N., Bohlin, R. C., Stecher, T. P., & Graff, S. M. 1987, *ApJ*, 321, 912
- Witt, A. N., Lindell, R. S., Block, D. L., & Evans, R. 1994, *ApJ*, 427, 227

Figure Captions

Figure 1— Broadband energy distribution (*filled circles*) of nebular surface brightness from NGC 2071, 30"E 30"S of the central star, together with the spectrum near the 3.3 μm emission feature (*histogram*). The 3.2–3.6 μm spectrum was measured with a circular variable filter with a spectral resolution $\lambda/\Delta\lambda = 67$ and a 10.5" diameter beam. Units are νS_ν in $\text{W m}^{-2} \text{sr}^{-1}$, where ν is the frequency and S_ν is the surface brightness at that frequency, and wavelength in μm . Uncertainties are $\pm 1\text{-}\sigma$. The data at J , H , K , L' , and near the 3.3 μm feature are from this paper. Visual data are from Witt & Schild (1986). An estimate of the surface brightness of scattered starlight (see text), normalized at V , is shown assuming either (*solid line*) the albedo is independent of wavelength or (*dotted line*) the albedo depends on wavelength as predicted by Draine & Lee (1984).

Figure 2— Near infrared colors $J - H$ and $H - K$ of extended emission in reflection nebulae. Nebulae in which the 3.3 μm emission feature was detected (*filled circles*), are plotted separately from nebulae (*open circles*) in which the 3.3 μm emission feature was not searched for, or searched for and not detected. The near infrared colors of the central stars with (*filled stars*) and without (*open stars*) hydrogen emission lines are also shown. Uncertainties shown are $\pm 1\text{-}\sigma$; no uncertainties are shown for the stellar colors. No limits on nebular colors are shown but they are consistent with the other nebular colors shown.

Figure 3— $V - K$ color of extended emission in reflection nebulae, $(V - K)_{\text{neb}}$, plotted vs. the $V - K$ color of the illuminating star, $(V - K)_{\text{star}}$. Nebulae in which the 3.3 μm emission feature was detected (*filled circles*), are plotted separately from nebulae (*open circles*) in which the 3.3 μm emission feature was not searched for, or searched for and not detected. The $V - K$ colors of the purely scattered light component in NGC 7023 (Paper IV) are also shown (*open triangles*). Upper limits are $3\text{-}\sigma$; uncertainties shown are $\pm 1\text{-}\sigma$. $(V - K)_{\text{neb}}$ as a function of $(V - K)_{\text{star}}$, predicted for scattered starlight (see text), is shown for four cases with different assumptions about how the albedo depends on wavelength and whether the nebula is optically thin or thick: (1) optically thick nebula, high albedo grains (*dotted line*); (2) optically thick nebula, low albedo grains (*short-dashed line*); (3) optically thin nebula, high albedo grains (*long-dashed line*); and (4) optically thin nebula, low albedo grains (*solid line*). Nebulae with K emission in excess of scattered starlight fall above and to the left of these lines.

Figure 4— Plot of the logarithm of the ratio of the observed K surface brightness, S_{obs} , to the estimated surface brightness of reflected starlight, $S_{\text{ref}}(\text{est})$, vs. $\log(T_{\text{star}})$, where T_{star} is the temperature of the central star of each nebula. Nebulae in which the 3.3 μm emission feature was detected (*filled circles*), are plotted separately from nebulae (*open*

circles) in which the $3.3 \mu\text{m}$ emission feature was not searched for, or searched for and not detected. Upper limits are $3\text{-}\sigma$. The purely scattered light component of the K emission of NGC 7023 (Paper IV) is also shown (*open triangles*). The uncertainty in $S_{\text{ref}}(\text{est})$ is a factor of 3, corresponding to an uncertainty in $\log[S_{\text{ref}}(\text{est})]$ of 0.5. Sources falling above the dotted line by more than this uncertainty likely have excess K emission due to something other than reflected starlight.

Figure 5— The strength of the $3.3 \mu\text{m}$ emission feature in reflection nebulae vs. temperature of the central star, T_{star} . Upper and lower limits are $3\text{-}\sigma$; uncertainties shown are $\pm 1\text{-}\sigma$. *Top*: K magnitude minus the magnitude at $3.3 \mu\text{m}$. The $3.3 \mu\text{m}$ magnitude includes both $3.3 \mu\text{m}$ continuum emission and any $3.3 \mu\text{m}$ feature emission. *Bottom*: The surface brightness (MJy sr^{-1}) at the peak of the $3.3 \mu\text{m}$ feature ratioed to the continuum surface brightness (MJy sr^{-1}) at $3.3 \mu\text{m}$. The $3.3 \mu\text{m}$ feature emission has been corrected for the continuum emission at $3.3 \mu\text{m}$, by interpolating between the K and L' surface brightnesses.

Figure 6— The surface brightness (MJy sr^{-1}) at the peak of the $3.3 \mu\text{m}$ feature ratioed to the continuum surface brightness (MJy sr^{-1}) at $3.3 \mu\text{m}$, vs. the $K - L'$ color. The $3.3 \mu\text{m}$ feature emission has been corrected for the continuum emission at $3.3 \mu\text{m}$, by interpolating between the K and L' surface brightnesses. Upper and lower limits are $3\text{-}\sigma$; uncertainties shown are $\pm 1\text{-}\sigma$.

Figure 7— Near infrared colors $J - H$, $H - K$ and $K - L'$ of extended emission in reflection nebulae plotted vs. temperature of the central star, T_{star} . Nebulae in which the $3.3 \mu\text{m}$ emission feature was detected (*filled circles*), are plotted separately from nebulae (*open circles*) in which the $3.3 \mu\text{m}$ emission feature was not searched for, or searched for and not detected. Uncertainties shown are $\pm 1\text{-}\sigma$. The $3\text{-}\sigma$ upper limits are given only for $K - L'$; the lower limits to $J - H$ and $H - K$ are consistent with the other plotted points.

Figure 1

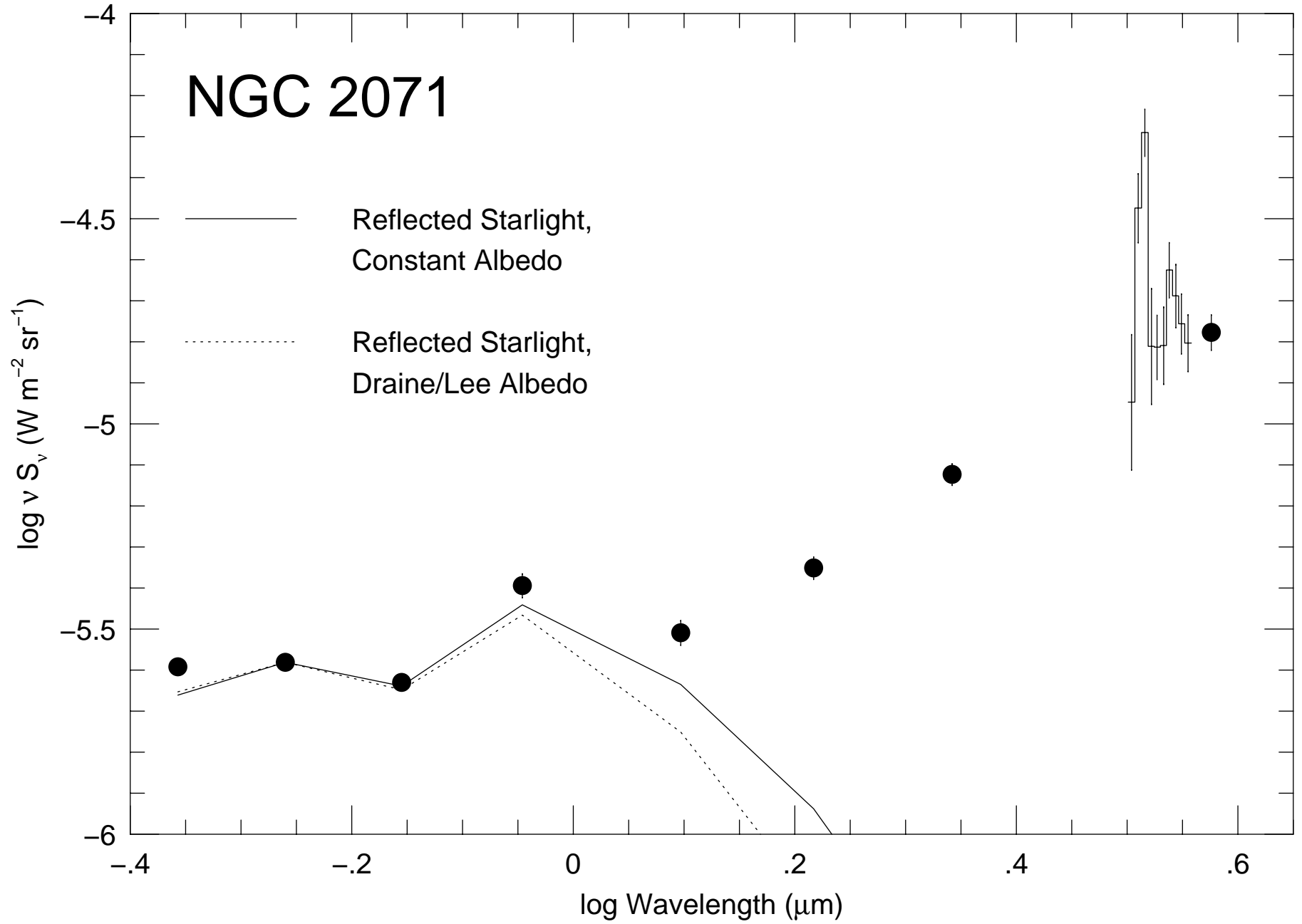


Figure 2

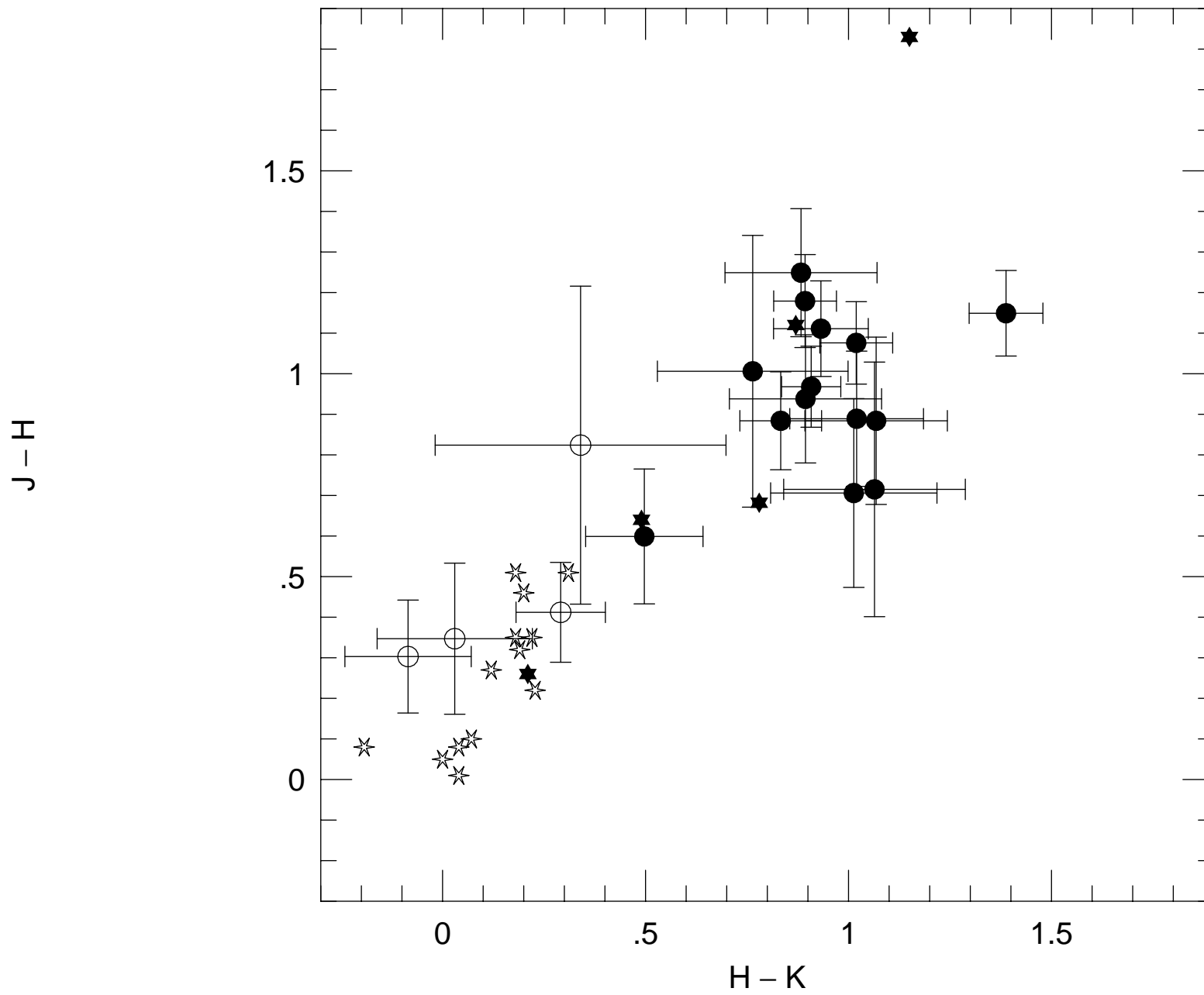


Figure 3

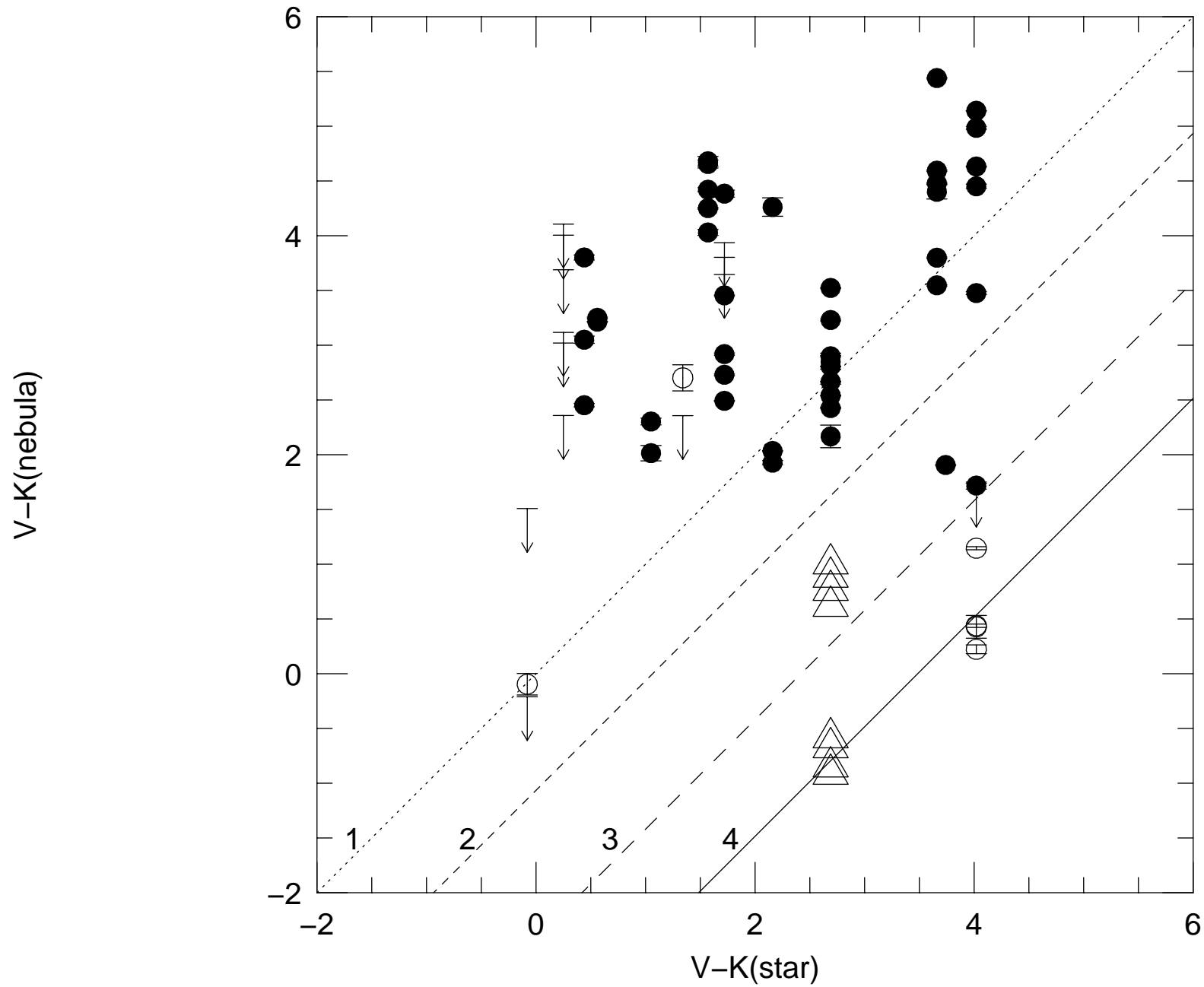


Figure 4

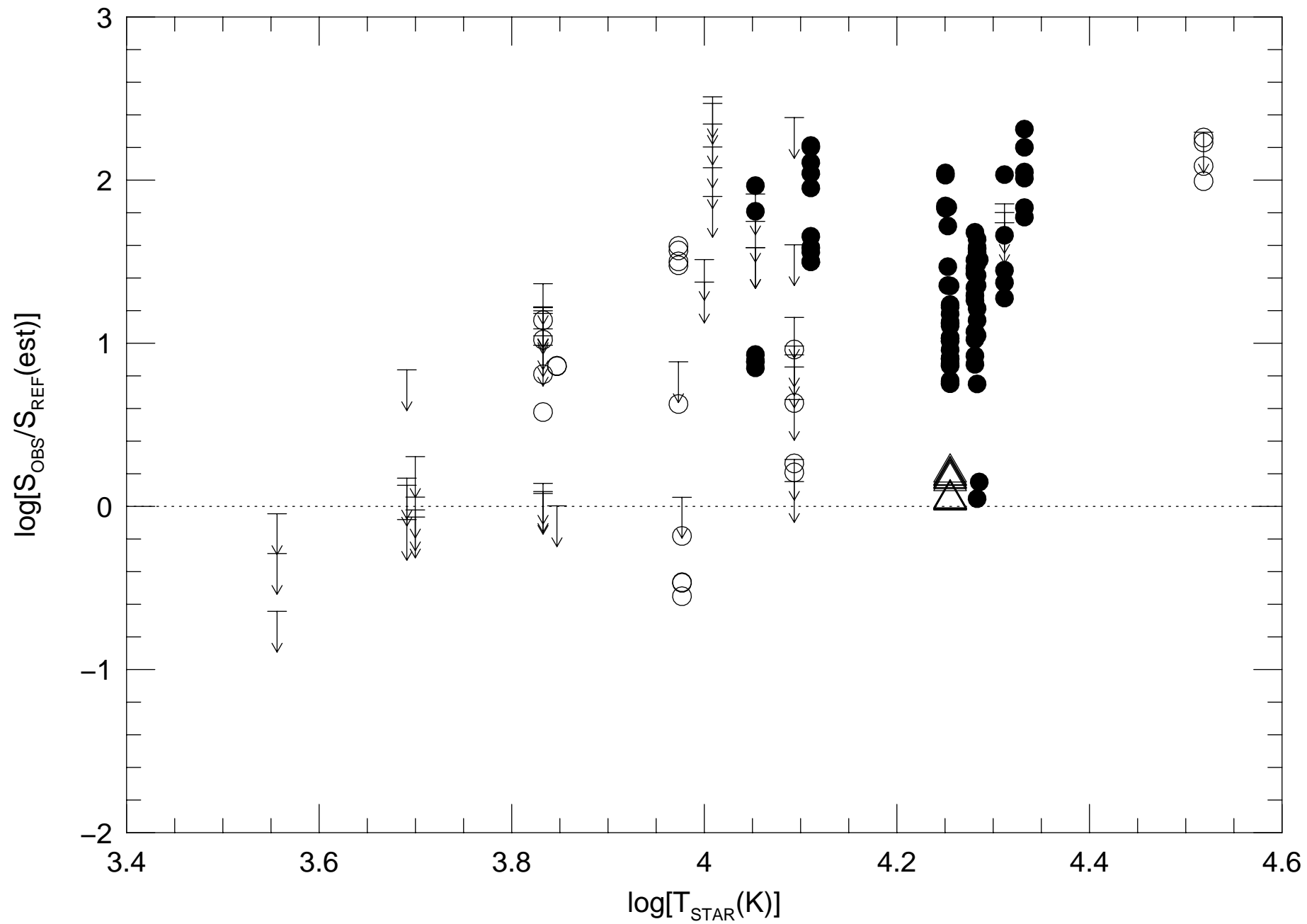


Figure 5

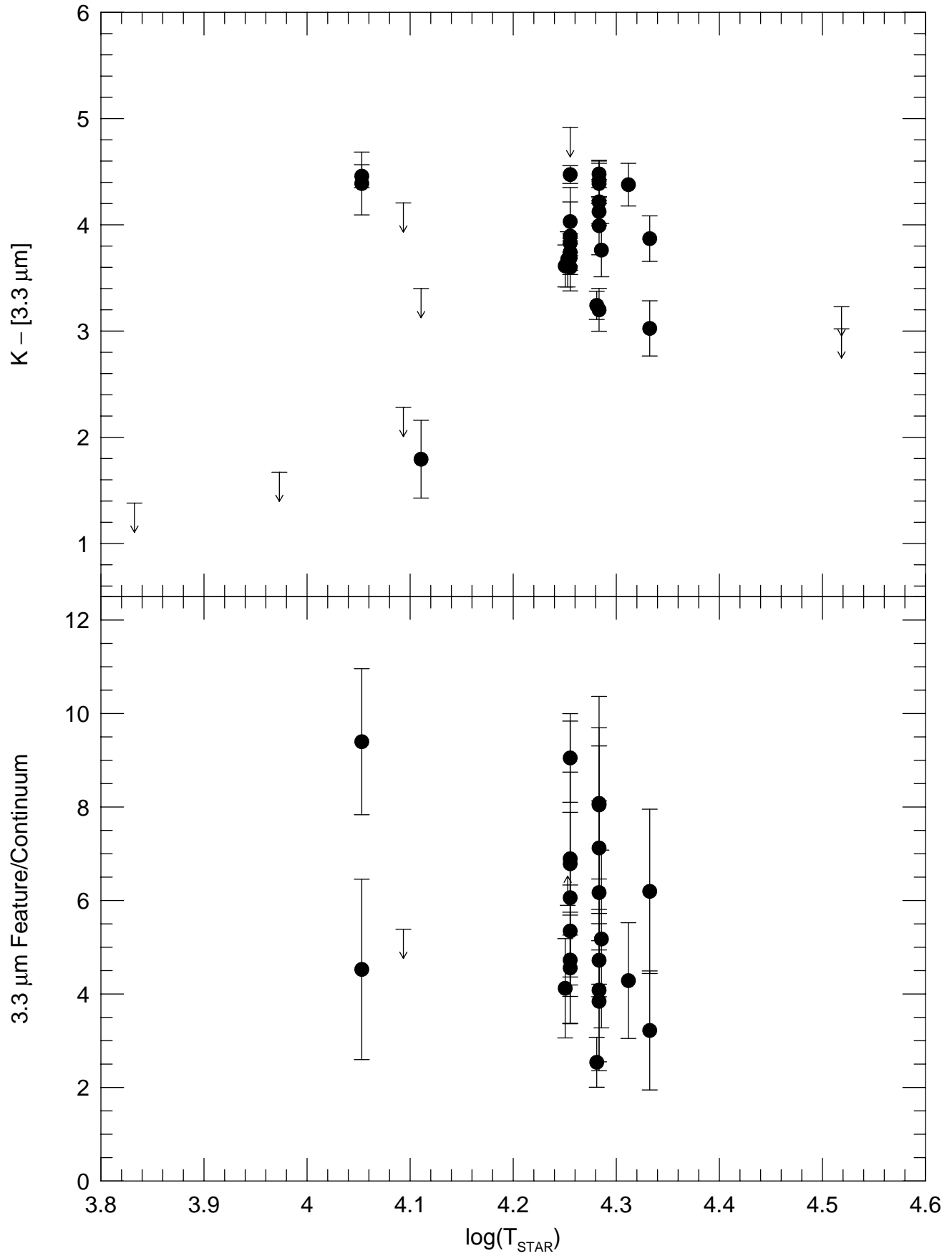


Figure 6

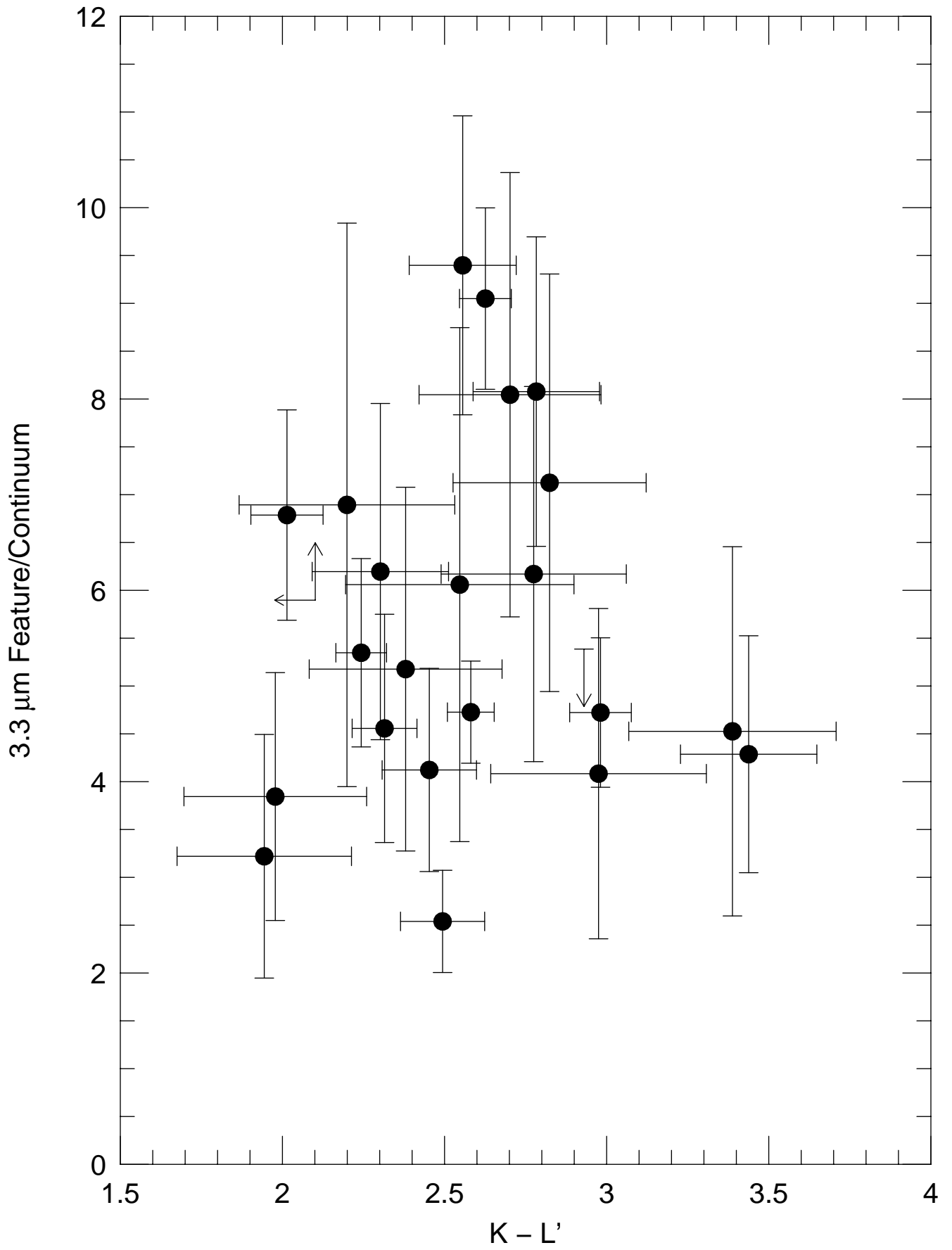


Figure 7

